



**HAL**  
open science

## **PHO1 family members transport phosphate from infected nodule cells to bacteroids in *Medicago truncatula***

Nga N T Nguyen, Joaquin Clua, Pallavi V Vetal, Dominique Jacques Vuarambon, Damien de Bellis, Marjorie Pervent, Marc Lepetit, Michael Udvardi, Alexander J Valentine, Yves Poirier

► **To cite this version:**

Nga N T Nguyen, Joaquin Clua, Pallavi V Vetal, Dominique Jacques Vuarambon, Damien de Bellis, et al.. PHO1 family members transport phosphate from infected nodule cells to bacteroids in *Medicago truncatula*. *Plant Physiology*, 2021, 185 (1), pp.196-209. 10.1093/plphys/kiab016 . hal-03274481

**HAL Id: hal-03274481**

**<https://hal.inrae.fr/hal-03274481>**

Submitted on 30 Jun 2021

**HAL** is a multi-disciplinary open access archive for the deposit and dissemination of scientific research documents, whether they are published or not. The documents may come from teaching and research institutions in France or abroad, or from public or private research centers.

L'archive ouverte pluridisciplinaire **HAL**, est destinée au dépôt et à la diffusion de documents scientifiques de niveau recherche, publiés ou non, émanant des établissements d'enseignement et de recherche français ou étrangers, des laboratoires publics ou privés.



Distributed under a Creative Commons Attribution 4.0 International License

# PHO1 family members transport phosphate from infected nodule cells to bacteroids in *Medicago truncatula*

Nga N.T. Nguyen,<sup>1</sup> Joaquin Clua ,<sup>1</sup> Pallavi V. Vetal ,<sup>1</sup> Dominique Jacques Vuarambon,<sup>1</sup> Damien De Bellis ,<sup>1,2</sup> Marjorie Pervent,<sup>3</sup> Marc Lepetit ,<sup>3</sup> Michael Udvardi ,<sup>4</sup> Alexander J. Valentine <sup>5</sup> and Yves Poirier <sup>1,\*†</sup>

- 1 Department of Plant Molecular Biology, Biophore Building, University of Lausanne, Lausanne 1015, Switzerland
- 2 Electron Microscopy Facility, Biophore Building, University of Lausanne, Lausanne 1015, Switzerland
- 3 Laboratoire des Symbioses Tropicales et Méditerranéennes UMR 1342 INRAE-IRD-CIRAD-UM-Montpellier SupAgro, Montpellier, France
- 4 The Noble Research Institute, 2510 Sam Noble Parkway, Ardmore, OK, USA
- 5 Botany & Zoology Department, University of Stellenbosch, Matieland 7602, South Africa

\*Author for communication: yves.poirier@unil.ch

†Senior author.

N.N.T.N., A.J.V., and Y.P. conceived the project. J.C. and D.J.V. contributed to plant transformation and analysis of gene expression; P.V.V. and D.d.B. performed confocal and electron microscopy, respectively; M.J. and M.L. helped with measurement of nitrogen fixation; and M.U. contributed essential mutant plant lines. N.N.T.N. performed all other experiments. N.N.T.N. and Y.P. wrote the manuscript, and M.L., A.J.V., J.C., and M.U. read and provided essential manuscript feedback. All authors read and approved the final manuscript. Y.P. agrees to serve as the author responsible for contact and ensures communication.

The author responsible for distribution of materials integral to the findings presented in this article in accordance with the policy described in the Instruction for Authors (<https://academic.oup.com/plphys>) is: Yves Poirier (yves.poirier@unil.ch).

## Abstract

Legumes play an important role in the soil nitrogen availability via symbiotic nitrogen fixation (SNF). Phosphate (Pi) deficiency severely impacts SNF because of the high Pi requirement of symbiosis. Whereas *PHT1* transporters are involved in Pi uptake into nodules, it is unknown how Pi is transferred from the plant infected cells to nitrogen-fixing bacteroids. We hypothesized that *Medicago truncatula* genes homologous to Arabidopsis *PHO1*, encoding a vascular apoplasmic Pi exporter, are involved in Pi transfer to bacteroids. Among the seven *MtPHO1* genes present in *M. truncatula*, we found that two genes, namely *MtPHO1.1* and *MtPHO1.2*, were broadly expressed across the various nodule zones in addition to the root vascular system. Expressions of *MtPHO1.1* and *MtPHO1.2* in *Nicotiana benthamiana* mediated specific Pi export. Plants with nodule-specific downregulation of both *MtPHO1.1* and *MtPHO1.2* were generated by RNA interference (RNAi) to examine their roles in nodule Pi homeostasis. Nodules of RNAi plants had lower Pi content and a three-fold reduction in SNF, resulting in reduced shoot growth. Whereas the rate of <sup>33</sup>Pi uptake into nodules of RNAi plants was similar to control, transfer of <sup>33</sup>Pi from nodule cells into bacteroids was reduced and bacteroids activated their Pi-deficiency response. Our results implicate plant *MtPHO1* genes in bacteroid Pi homeostasis and SNF via the transfer of Pi from nodule infected cells to bacteroids.

Received August 24, 2020. Accepted October 14, 2020. Advance access publication November 25, 2020

© The Author(s) 2020. Published by Oxford University Press on behalf of American Society of Plant Biologists.

This is an Open Access article distributed under the terms of the Creative Commons Attribution-NonCommercial-NoDerivs licence

(<http://creativecommons.org/licenses/by-nc-nd/4.0/>), which permits non-commercial reproduction and distribution of the work, in any medium, provided the original work is not altered or transformed in any way, and that the work is properly cited. For commercial re-use, please contact [journals.permissions@oup.com](mailto:journals.permissions@oup.com)

Open Access

## Introduction

Biological fixation of nitrogen by rhizobia is of prime importance in the global nitrogen cycle and a major provider of fixed nitrogen in agricultural soils (Herridge et al., 2008). The rhizobia–legume interaction occurs within the nodule, a specialized root structure, whereby rhizobia fixes atmospheric nitrogen in exchange for organic acids and other nutrients provided by the plant (Udvardi and Poole, 2013). Rhizobia enters the root via an infection thread initiated within the root hairs that eventually reaches cortical cells that divide and multiply in response to Nod factors released by the bacteria (Oldroyd et al., 2011; Mergaert et al., 2020; Roy et al., 2020). Bacteria released from the infection thread enter the cortical cells via a process generating an organelle-like structure, the symbiosome, whereby the bacteria are surrounded by a membrane derived from the plant plasma membrane (PM). This membrane, named the peribacteroid or symbiosome membrane (SM), separate the bacteria, which ultimately differentiate into nitrogen-fixing bacteroids, from the plant cytosol (Whitehead and Day, 1997). Proteomic analysis of SM identified a range of transporters, pumps, and channels that are thought to contribute to the movement of nutrients and ions between the plant cells and the bacteroids (Saalbach et al., 2002; Wienkoop and Saalbach, 2003; Clarke et al., 2015). Despite this, our current knowledge of the proteins involved in the movement of specific nutrients and ions from the cytosol of infected nodule cells to the bacteroids is very limited. For example, whereas malate is thought to be the main source of carbon provided by the plant to the bacteroid in exchange for ammonia, the malate transporter involved in this exchange is still unknown (Clarke et al., 2014; Poole et al., 2018). However, proteins involved in the transport of nitrate and citrate to the bacteroids have been described (Vincill et al., 2005; Kryvoruchko et al., 2018).

Beyond carbon and nitrogen, the plant cell must also provide bacteroids with numerous elements essential for proper metabolism, including calcium, sulfate ( $\text{SO}_4$ ), potassium, and several metals such as iron, zinc, and copper. *Glycine max* ZIP1 and DMT1 were shown to be transporters for zinc and iron, respectively, when synthesized in yeast, and found to be expressed in nodules and localized to the SM (Moreau et al., 2002; Kaiser et al., 2003). Similarly, a protein from *Lotus japonicus* that can mediate  $\text{SO}_4$  transport when expressed in yeast was shown to be essential for symbiotic nitrogen fixation (SNF; Krusell et al., 2005).

Phosphorus (P) is one of the most limiting nutrients for plant growth, especially in legumes that can access atmospheric nitrogen via SNF. P level in soybean nodules are 3-fold higher than in roots and leaves (Gaude et al., 2004) and legumes require higher levels of P for growth supported by SNF compared to growth on nitrate (Israel, 1987, 1993; Gunawardena et al., 1992). Nodules are highly active metabolically, with protein concentrations more than an order of magnitude higher than in roots (Gaude et al., 2004). The

comparison of phosphorylated metabolites in free living *Bradyrhizobium japonicum* and bacteroids isolated from soybean nodules showed a large increase in P-containing metabolites in bacteroids, ranging from free inorganic phosphate (Pi) to ATP and numerous phosphorylated intermediates (Vauclare et al., 2013). Pi deficiency can affect SNF either indirectly, e.g. by reducing photosynthesis and carbon supply from the plant to the bacteroids, or directly by constraining nodule development and metabolic activity through its impact on Nod factor production and nitrogenase activity (McKay and Djordjevic, 1993; Hernandez et al., 2009). Adaptation of legumes to Pi deficiency shares many similarities to that of nonleguminous plants, including changes in root development, secretion of organic acids and phosphatases into the rhizosphere, and the activation of pathways that bypass the need for ATP and some P-containing compounds (O'Rourke et al., 2013; Sulieman and Tran, 2015). The main Pi-deficiency signaling components identified in Arabidopsis, including the transcription factor PHR1, the small RNA mi399, and SPX signaling components, are also found in legumes (Xu et al., 2013; Zhang et al., 2016; Xue et al., 2017). Nevertheless, it is likely that adaptation of nodules to Pi deficiency allowing the maintenance of nitrogen fixation involves nodule-specific mechanisms (Valentine et al., 2017).

Plants acquire P from their environment via Pi transporters coupled to a proton gradient generated by  $\text{H}^+$ -ATPases associated with the PM. The principal transporters of Pi into plant cells belong to the PHT1 family (Nussaume et al., 2011; Poirier and Jung, 2015). Two pathways for Pi entry into nodules have been described, namely a direct uptake by the nodule and an indirect pathway involving Pi transfer from roots of the host plant to the nodule (Al-Niemi et al., 1998). Expression of two PHT1 genes in soybean nodules was shown to be essential for nodulation and nitrogen fixation, highlighting their implication in the uptake of Pi into nodules (Qin et al., 2012; Chen et al., 2019). Whereas entry of Pi into bacteroids is mediated by low-affinity Pit- and high-affinity Pst bacterial Pi transporters (Bardin et al., 1998; Botero et al., 2000; Yuan et al., 2006), plant transporters required to transfer Pi from the host cell cytoplasm to the bacteroids are unknown.

The *Arabidopsis thaliana* and rice (*Oryza sativa*) AtPHO1 and OsPHO1.2 genes are involved in loading of Pi into the xylem vessel for transfer to the shoot (Hamburger et al., 2002; Secco et al., 2010). AtPHO1 is also expressed in the chalazal seed coat where it is involved in the transfer of Pi from the maternal seed coat to the filial developing embryo (Vogiatzaki et al., 2017). AtPHO1 expressed in Arabidopsis or *N. benthamiana* mediates Pi export across the PM to the apoplastic space (Arpat et al., 2012; Wege et al., 2016). Given the role of AtPHO1 in Pi transfer between tissues, we hypothesized that homologues of PHO1 in legumes could be involved in Pi homeostasis in the nodule, and more specifically in

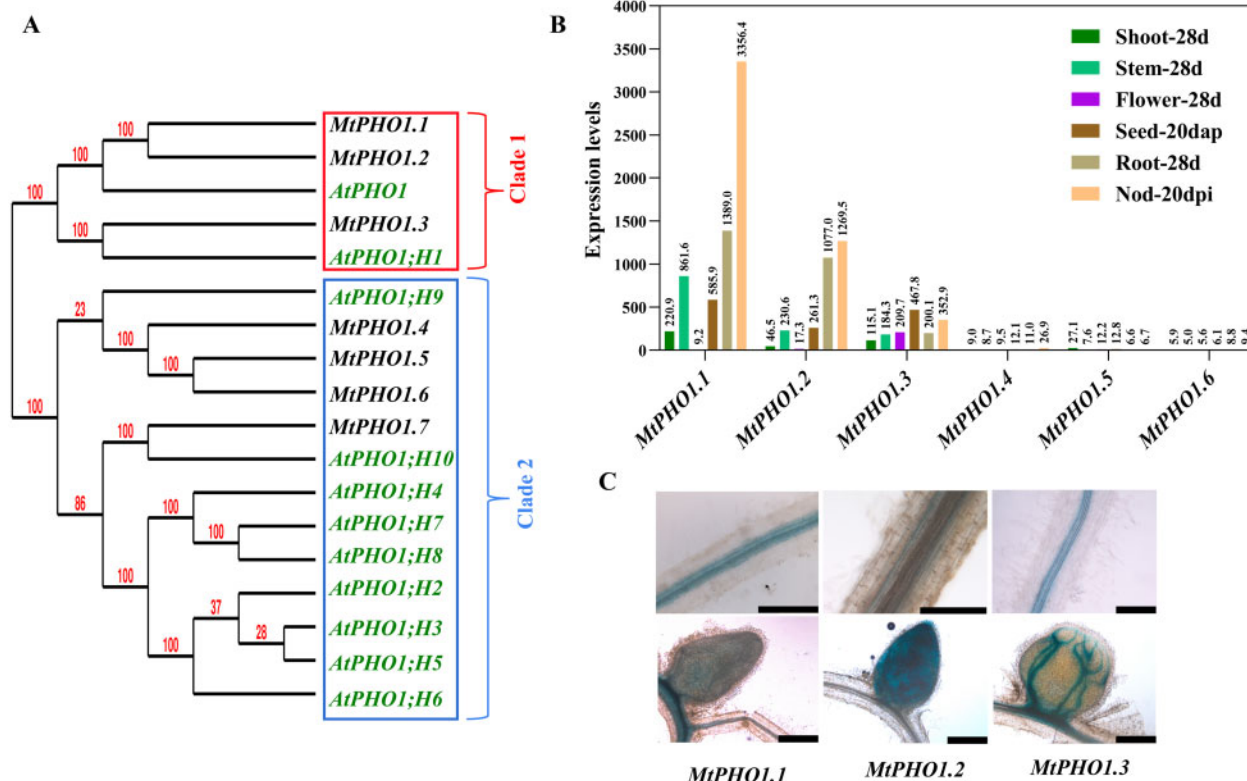


**Figure 1** Phylogeny and expression of the *PHO1* family in *M. truncatula*. (A) Unrooted phylogenetic tree of *PHO1* from *Arabidopsis* (green) and *M. truncatula* (black) showing the two main clades. Numbers at the nodes indicates the bootstrap values on neighbor joining analysis. (B) Expression of the *M. truncatula PHO1* genes obtained from the *M. truncatula* Gene Expression Atlas using an Affymetrix Medicago Gene Chip and RNA isolated from shoots, stems, flowers, and roots from 28-d-old plants (28 d), seeds 20 d after pollination (20 dap), and nodules 20 d after inoculation (20 dpi) with *S. meliloti* (mtgea.noble.org/v3/). The tissues analyzed are indicated by a color code (top right corner) and the order is kept the same for all genes. (C) GUS staining in *M. truncatula* roots (upper panels) and nodules (lower panels) transformed with promoter:cDNA-GUS fusions for the *M. truncatula* genes *MtPHO1.1*, *MtPHO1.2*, and *MtPHO1.3*. Bars represent 200  $\mu\text{m}$ .

Pi transfer to the bacteroid. In this work, we characterize the *PHO1* gene family in *M. truncatula* and report the role of two *MtPHO1* transporters in the transfer of Pi from infected plant cells to the bacteroids.

## Results

### Identification of *MtPHO1* genes expressed in nodules

Seven genes encoding proteins with high similarity to *AtPHO1*, including conserved SPX and EXS domains, were identified using the TBLASTN function of the *M. truncatula* Genome Database (<http://blast.jcvi.org/Medicago-Blast/index.cgi>; Supplemental Figure S1). Phylogenetic analysis grouped the *MtPHO1* homologs into two distinct clades, in agreement with previous analysis of the *PHO1* gene family in monocots and dicots (Secco et al., 2010). Clade 1 contains three *M. truncatula PHO1* homologs, named *MtPHO1.1–1.3*, whereas four genes named *MtPHO1.4–1.7* belong to clade 2 (Figure 1A).

The expression profiles of *MtPHO1* genes was assessed using the *M. truncatula* Gene Expression Atlas (mtgea.noble.org/v3/) compiling data obtained using a dedicated Affymetrix Medicago Gene Chip (affymetrix.com) that

contained probes for six *MtPHO1* genes, namely *MtPHO1.1–1.6*. The three *MtPHO1* genes belonging to clade 1, namely *MtPHO1.1*, *MtPHO1.2*, and *MtPHO1.3*, were broadly expressed in the shoot, stem, flower, seed, root, and nodule, with *MtPHO1.1* and *MtPHO1.2* being the genes expressed most robustly in nodules (Figure 1B). In contrast, *MtPHO1.4–1.6* genes were not expressed, or only very weakly, in various tissues, including nodules. Reverse transcription–polymerase chain reaction (RT–PCR) analysis of nodules from *M. truncatula* inoculated with *Sinorhizobium meliloti* and grown under nitrogen-fixing conditions confirmed the expression of *MtPHO1.1*, *MtPHO1.2*, and *MtPHO1.3*, whereas expression of all other genes, including *MtPHO1.7*, was either very weak or undetectable (Supplemental Figure S1B). The genomic structure of the *MtPHO1.1* and *MtPHO1.2* loci as well as *MtPHO1.1* and *MtPHO1.2* amino-acid alignment with the *A. thaliana PHO1* are shown in Supplemental Figure S1.

The spatial expression patterns of the three main *MtPHO1* genes expressed in nodules was investigated further by gene-GUS fusion analysis (Figure 1C). All constructs included a 2-kb promoter region and the cDNA sequence of *MtPHO1.1*, *MtPHO1.2*, or *MtPHO1.3* fused at

the C-terminus to the *uidA* gene, and histochemical analysis for GUS activity was performed on roots and nodules from composite transgenic plants grown under nitrogen-fixing conditions. All three genes were expressed in the vascular cylinder of roots (Figure 1C, upper panels). Whereas GUS staining for the *pMtPHO1.3:cMtPHO1.3-GUS* construct was detected only in the vascular tissue in nodules, GUS expression from the *pMtPHO1.1:cMtPHO1.1-GUS* and *pMtPHO1.2:cMtPHO1.2-GUS* constructs was not limited to the vascular tissue but observed across the whole nodule (Figure 1C, lower panels). Since transporters involved in Pi transfer from the infected cortical cells to the bacteroids are expected to be broadly expressed in cells of the nodule and not be confined to the vascular cylinder, further analysis was restricted to the *MtPHO1.1* and *MtPHO1.2* genes. Analysis of the expression patterns of these two genes using data from the Symbimics database (<https://iant.toulouse.inra.fr/symbimics>), derived from laser-capture microdissection of nodules (Roux et al., 2014), confirmed that both genes were broadly expressed in the nodules, from the meristematic zone to the nitrogen-fixing zone (Supplemental Figure S2).

### *MtPHO1.1* and *MtPHO1.2* are Pi exporters

Pi transport activity of the *MtPHO1.1* and *MtPHO1.2* proteins fused to GFP was tested by transient expression in *N. benthamiana* leaves. Arabidopsis PHO1-GFP and free GFP were expressed as positive and negative controls, respectively. Transient expression of *MtPHO1.1-GFP* and *MtPHO1.2-GFP* fusions led to greater export of Pi into the extracellular medium than either free GFP or noninfiltrated controls, and to a similar extent to the expression of the Arabidopsis PHO1-GFP (Figure 2A). In contrast, nitrate export was unaffected by expression of any of these transporters, indicating specificity for Pi export of *MtPHO1.1* and *MtPHO1.2*.

Expression of *MtPHO1.1-GFP* and *MtPHO1.2-GFP* fusion proteins in *M. truncatula* hairy root transformants using the gene's endogenous promoters did not show reliable GFP expression above the autofluorescence background in either nodules or root vascular cylinder. Subcellular localization of *MtPHO1.1-GFP* and *MtPHO1.2-GFP* was thus determined by transient expression in *N. benthamiana*. *MtPHO1.1-GFP* or *MtPHO1.2-GFP* was co-expressed with either the Golgi marker ManI-RFP (Langhans et al., 2011) or the PM marker CBL1-OFP (Batistič et al., 2010). AtPHO1-GFP has previously been shown to colocalize with the Golgi marker (Arpat et al., 2012), and a similar co-localization occurred with the *MtPHO1.2-GFP* construct. In contrast, *MtPHO1.1-GFP* co-localized primarily with the PM marker and not with the Golgi marker (Figure 2B).

### *MtPHO1.1* and *MtPHO1.2* contribute to nitrogen fixation

In order to identify roles of *MtPHO1.1* and *MtPHO1.2* in nodulation and nitrogen fixation, *M. truncatula* mutants for each gene were obtained from the *Transposable Element*

from *N. tabacum* (*Tnt1*) collection of the Noble Research Institute (Tadege et al., 2008). Two homozygous mutant lines for each gene were identified and evaluated. Mutants *mtpho1.1a* (NF14242) and *mtpho1.1b* (NF14056) harbor *Tnt1* insertions in the second and seventh introns of the *MtPHO1.1* gene, respectively, leading to an approximately 50%–60% reduction in gene expression levels (Figure 3, A and C). The two independent mutants *mtpho1.2a* (NF1102) and *mtpho1.2b* (NF10573) contain *Tnt1* insertions in the first and second exons, respectively, and resulted in undetectable levels of gene expression (Figure 3, A and C). Growth of all four *Tnt1* mutants under nitrogen-fixing conditions were undistinguishable from either the parental R108 or WT segregants obtained from the heterozygous mutants, with no significant change in either shoot fresh weight or Pi content of shoot or nodule, nodule number or nodule size (Figure 3, B, D–H).

Because of the potential functional redundancy between *MtPHO1.1* and *MtPHO1.2*, we aimed to create transgenic lines where both genes are downregulated. Since both *MtPHO1.1* and *MtPHO1.2* are not only expressed in nodules but also various other tissues, including in the vascular cylinder of roots, we chose to downregulate the expression of both genes specifically in nodules with an RNAi approach using the nodule-specific promoter of the *NCR001* gene (Mergaert et al., 2003). Three distinct hairpin RNAi constructs were designed using sequences outside the PHO1 SPX and EXS domains, corresponding to regions of highest divergence between members of the *MtPHO1* family (Supplemental Figure S3A). Each RNAi construct was a hybrid containing ~500 bp of coding sequence of both *MtPHO1.1* and *MtPHO1.2* genes, and thus designed to downregulate both genes simultaneously (Supplemental Figure S4). Composite plants with transgenic roots expressing the RNAi construct or transformed with an empty vector (EV) control were inoculated with *S. meliloti* and grown in a clay-based substrate in the presence of either full nutrient containing a source of nitrogen ( $\text{NO}_3$  and  $\text{NH}_4\text{NO}_3$ ) or full nutrient without mineral nitrogen. Several independent composite transgenic plants transformed with each of the three RNAi constructs gave plants that grew poorly under mineral nitrogen-free conditions compared to EV controls (Supplemental Figure S3B). These plants exhibited shoot Pi content comparable to EV controls but had lower nodule Pi contents and nodules had significantly higher fresh weights than those of controls (Supplemental Figure S3, C–E). Because the phenotypes observed with the three RNAi constructs were similar, further detailed characterization of the RNAi phenotype was limited to composite plants transformed with the RNAi3 construct (Figure 4).

Reverse transcription quantitative PCR (RT-qPCR) analysis of transgenic roots transformed with RNAi3 showed an approximate 55% reduction in *MtPHO1.1* and *MtPHO1.2* expression; however, this was confined to nodules and gene expression in root sections without nodules was unchanged

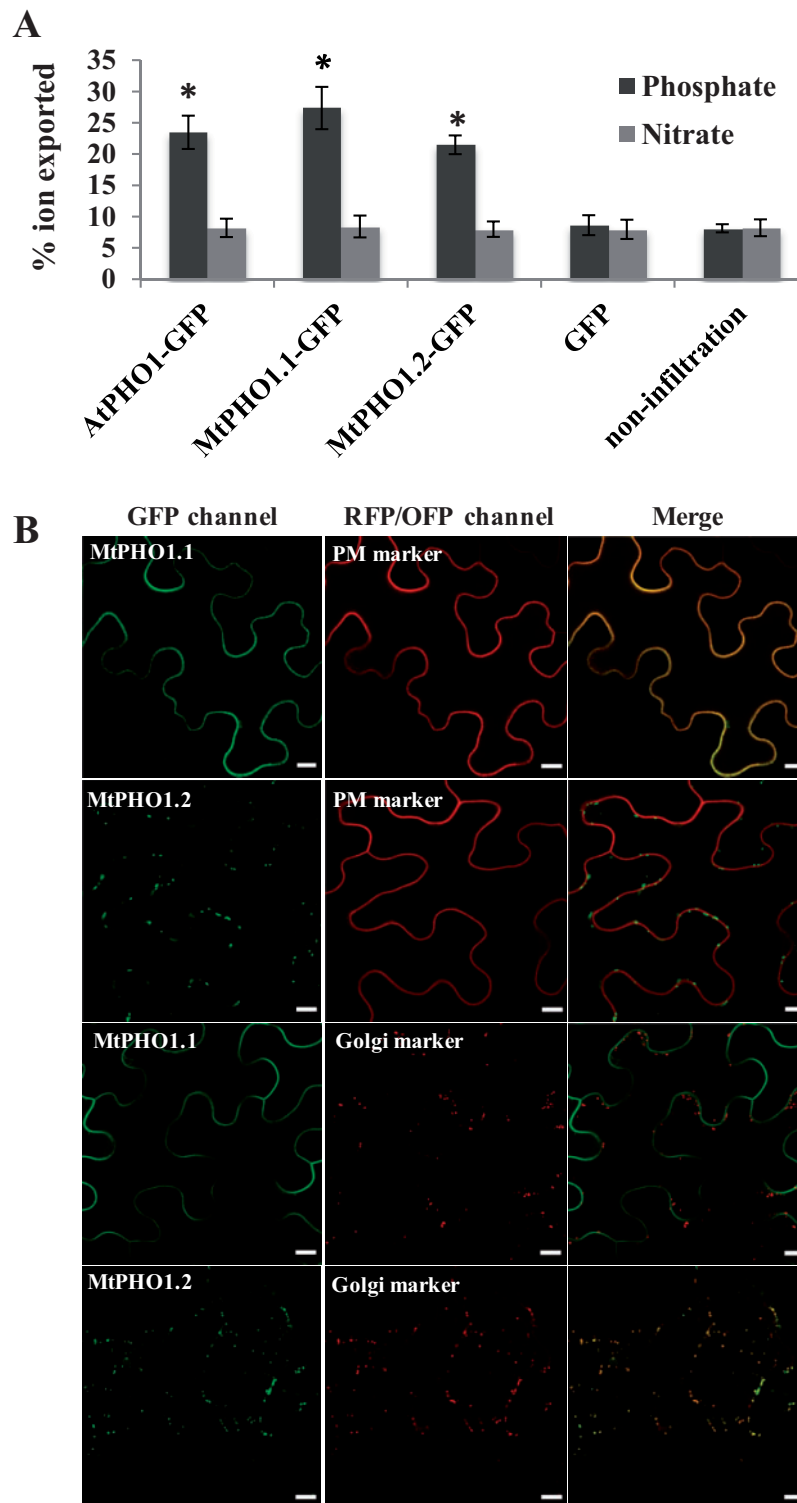


**Figure 2** *MtPHO1.1* and *MtPHO1.2* genes mediate Pi export. **(A)** Measurement of Pi and nitrate export mediated by the transient expression in *N. benthamiana* leaf discs of the Arabidopsis PHO1-GFP, or *M. truncatula* PHO1.1-GFP and PHO1.2-GFP fusion proteins. As controls, Pi and nitrate export were measured in leaf discs expressing either free GFP or not infiltrated. Error bars represent *SD* ( $n = 4$ ). Values on the *y*-axis represent the percentage of total ion present in the tissue at time 0 that is exported in the medium after 2 h. Asterisks represent statistically significant differences compared to the GFP or noninfiltrated control (*t* test,  $P < 0.05$ ). **(B)** Subcellular localization of *MtPHO1.1*-GFP and *MtPHO1.2*-GFP fusion proteins transiently expressed in *N. benthamiana*. *MtPHO1.1*-GFP and *MtPHO1.2*-GFP were co-expressed with the PM marker CBL1-OFP (upper two panels) and the Golgi marker Man1-RFP (lower two panels). Scale bars = 10  $\mu\text{m}$ .

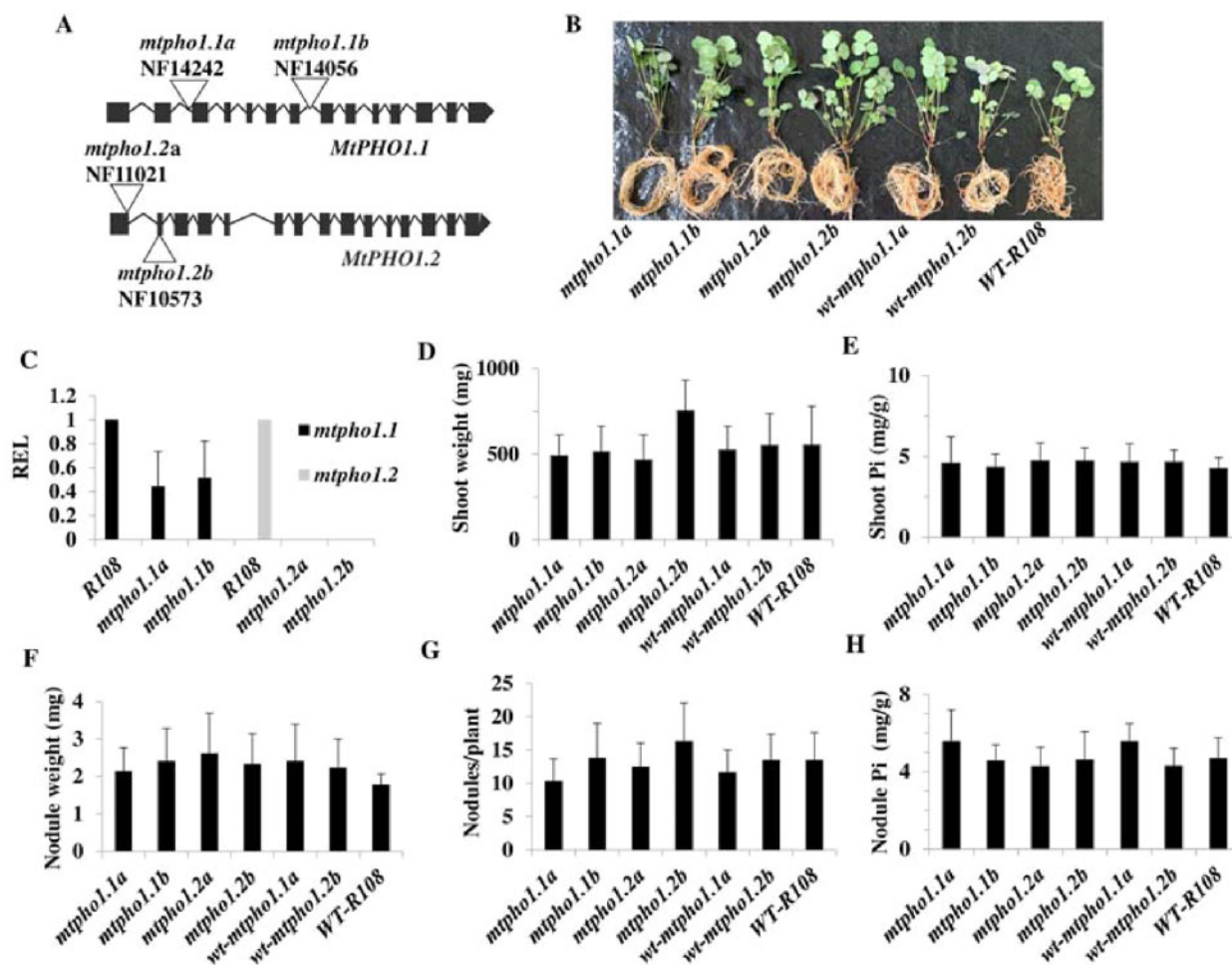


**Figure 3** Analysis of *MtPHO1.1* and *MtPHO1.2* insertion mutants. (A) Localization of *Tnt1* insertions within the *MtPHO1.1* and *MtPHO1.2* genes. Black boxes and lines represent exons and introns, respectively. (B) Visual appearance of *Tnt1* mutant plants and controls when grown for 28 d under SNF conditions. Control plants were either the R108 genotype or WT-segregants derived from heterozygous *Tnt1* mutant lines. C, Expression level of the *MtPHO1.1* and *MtPHO1.2* genes in the various *Tnt1* mutants relative to the WT control R108 (set at 1) as detected by RT-qPCR. REL, relative expression level. Error bars represent *sd* ( $n = 3$ ). Measurement of shoot fresh weight (D), shoot Pi content (E), nodule fresh weight (F), number of nodules per plants (G), and nodule Pi content (H) in plants grown in clay-based soil under SNF conditions for 28 d. For (D–H), error bars represent *sd* ( $n \geq 6$ ).

relative to the EV control (Figure 4A). The reduction in shoot fresh weight of the RNAi-transformed roots was only observed in plants grown under SNF conditions and not when plants were grown in the presence of a fixed nitrogen source in the nutrient solution (Figure 4, B and C). Under both growth conditions, shoot Pi content remained similar between RNAi and EV (Figure 4D). Although nodules from RNAi roots showed an increase in the fresh weight as compared to EV and contained less Pi per mass, the number of nodules per plant remained unchanged (Figure 4, E–G).

Nitrogen fixation in isolated nodules was measured using  $^{15}\text{N}_2$ . Plants with roots transformed with the RNAi3 construct showed a 3.5-fold reduction in the specific nitrogen fixation activity ( $\text{N}_2$  fixation per nodule biomass) relative to the EV control (Figure 4H). Although this reduction was partially compensated by an increase of nodule biomass in the RNAi plants, the reduced expression of

*MtPHO1.1* and *MtPHO1.2* specifically in nodules decreased the nitrogen fixation potential of the plant, resulting in reduced growth of plants in the absence of mineral nitrogen.

Nodules from roots transformed with the EV control or RNAi3 construct roots appeared similar in gross nodule structure (Figure 5A). However, bacteroids in the nitrogen fixation zone (zone 3) showed a significant reduction in cell length in nodules derived from RNAi roots compared to EV controls, as measured by electron microscopy (Figure 5, B and C).

### Reduction of *MtPHO1.1* and *MtPHO1.2* expression results in Pi-deficient bacteria

The dynamics of Pi and  $\text{SO}_4$  entry into nodules and its transfer to bacteroids were measured using radio-isotopes. Excised nodules from roots transformed with the RNAi3

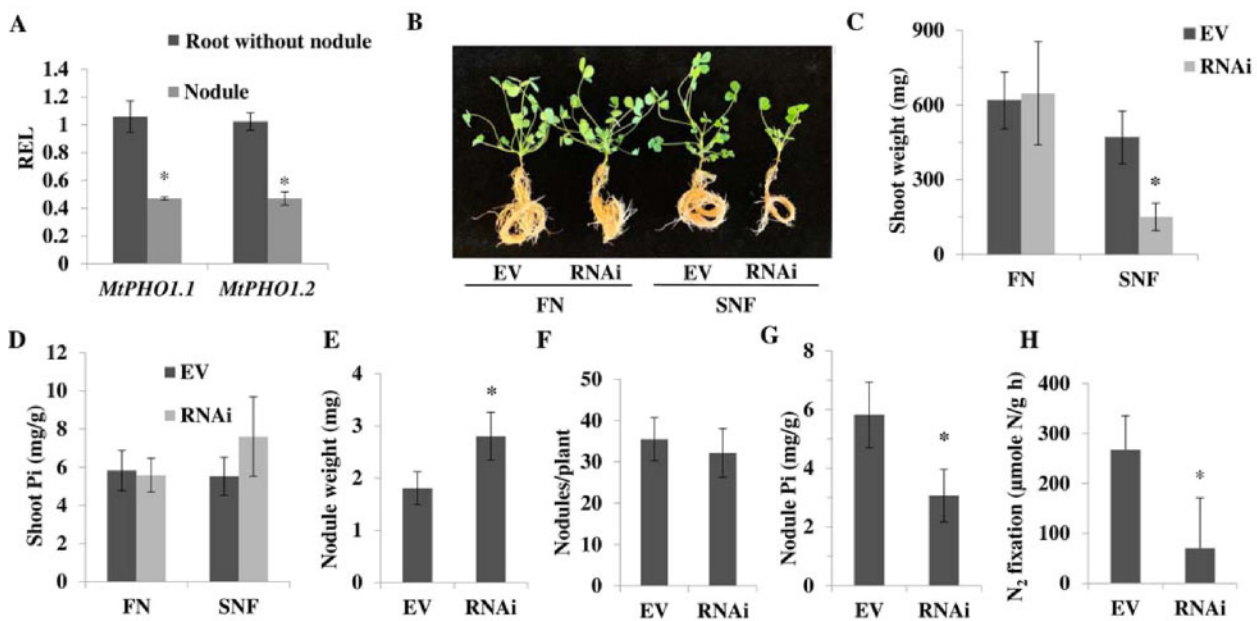


**Figure 4** Analysis of RNAi lines with reduced expression of *MtPHO1.1* and *MtPHO1.2* genes. **(A)** Expression level of the *MtPHO1.1* and *MtPHO1.2* genes in the nodules and sections of roots devoid of nodules relative to the EV control as detected by RT-qPCR. REL, relative expression level. Error bars represent SD ( $n = 3$ ). **(B)** Visual appearance of RNAi plants and EV controls for plants grown for 28 d in clay soil supplemented with full nutrient (FN) including nitrate and ammonium or grown under SNF conditions. Measurement of shoot fresh weight **(C)**, shoot Pi content **(D)**, nodule fresh weight **(E)**, number of nodules per plants **(F)**, nodule Pi content **(G)**, and nitrogen fixation activity of nodules **(H)** in plants grown in SNF conditions for 28 d. For **(C–H)** error bars represent SD ( $n \geq 6$ ). Asterisks represent statistically significant differences compared to the EV control ( $t$  test,  $P < 0.05$ ).

construct imported similar amounts of either  $^{33}\text{P}$  or  $^{35}\text{S}$  from the bathing solution compared to nodules from EV controls (Figure 6, A and B). However, there was a two-fold reduction in the amount of  $^{33}\text{P}$  acquired by bacteroids in the RNAi lines compared to EV controls, whereas the amount of  $^{35}\text{S}$  acquired by the bacteroids was not different between RNAi and EV-control root nodules (Figure 6C). These data indicated a deficiency in Pi transfer from plants cells to the bacteroids.

To test whether the bacteria present in nodules on roots transformed with the RNAi3 construct experienced Pi deficiency, we inoculated plants with the *S. meliloti* RCR2011 strain containing *pstS::gusA* or *orfa-pit::gusA* reporter genes. *PstS* encodes a high-affinity Pi transporter and its promoter is activated under Pi deficiency, whereas *Pit* encodes a low-affinity Pi transporter and is repressed under Pi deficiency (Yuan et al., 2006). Compared to the EV control, nodules from roots transformed with the RNAi3 construct containing *S. meliloti* with *orfa-pit::gusA* showed a decrease in GUS expression throughout the nodule whereas an increase in GUS expression was associated with *S. meliloti* expressing *pstS::gusA* in RNAi3-expressing nodules compared to the control (Figure 6D). Altogether, these experiments showed that downregulation of *MtPHO1.1* and *MtPHO1.2* expression was accompanied by a reduction of Pi transfer from infected nodule cells to bacteroids, resulting in Pi-deficient bacteroids and a reduction in nitrogen fixation.

## Discussion

Phylogenetics analysis of the *PHO1* gene family in angiosperms showed the presence of two major clades (Secco et al., 2010; He et al., 2013). Genes in Clade 1 are found in both monocots and dicots and include genes with highest homology to *AtPHO1* and *AtPHO1;H1*, the only two genes in *A. thaliana* shown to mediate Pi export to the root xylem vessels for long-distance Pi transport (Stefanovic et al., 2007). *PHO1*-like genes belonging to Clade 1 in rice and tomato (*Solanum lycopersicum*) are also involved in the long-distance transfer of Pi from roots to shoots (Secco et al., 2010; Zhao et al., 2019). By contrast, genes in Clade 2 are present only in dicots, and none have been shown to be directly involved in long-distance Pi transport (Stefanovic et al., 2007). The only functionally characterized members of this clade are *AtPHO1;H4* (*SHB1*), implicated in hypocotyl elongation in blue light (Kang and Ni, 2006); and *AtPHO1;H3*, thought to negatively modulate *AtPHO1* activity under zinc deficiency (Khan et al., 2014). *MtPHO1.1*, *MtPHO1.2*, and *MtPHO1.3* all belong to Clade 1 and are the only *M. truncatula* *PHO1* genes with robust expression in a range of tissues, including nodules. Similar to the Pi exporters *AtPHO1* and *AtPHO1;H1* in Arabidopsis and *OsPHO1.2* in rice (Hamburger et al., 2002; Stefanovic et al., 2007; Jabnourne et al., 2013), these three *M. truncatula* genes are expressed in the root vascular cylinder. These data, combined with the Pi export activity of *MtPHO1.1* and *MtPHO1.2* expressed in *N. benthamiana*, suggest that these genes are also likely involved in long-distance Pi transfer via Pi export into the xylem. Since the null *mtpho1.2* mutants showed

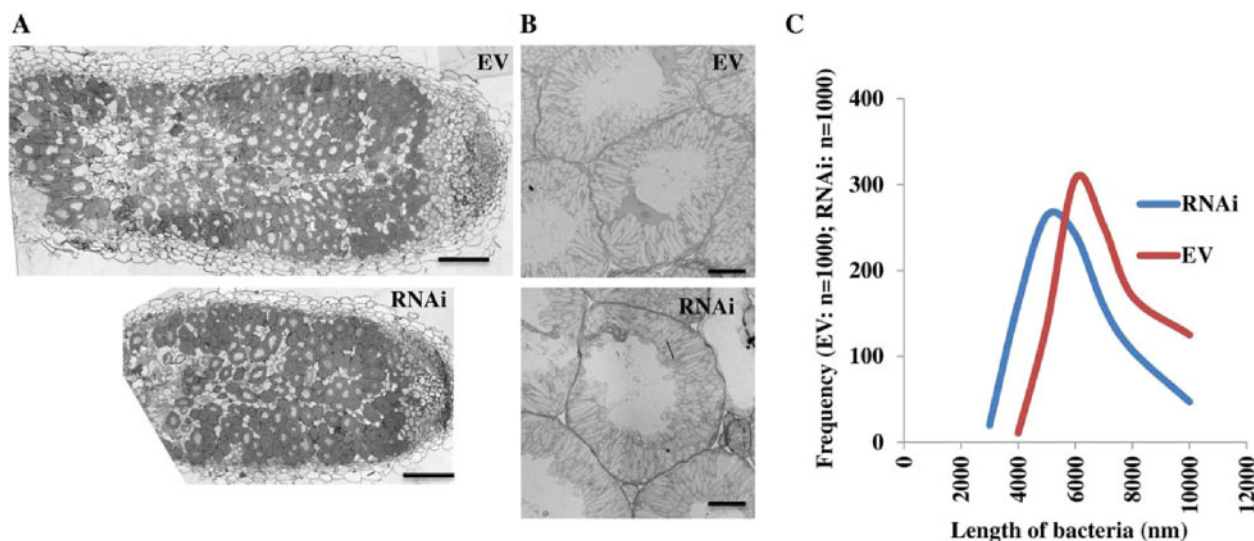


**Figure 5** Bacteroid size and distribution in nodules. (A) Panoramic reconstruction of  $3 \times 3$  and  $5 \times 5$  pictures showing a 200- $\mu\text{m}$ -thick longitudinal section of nodules from EV control and RNAi plants grown for 28 d under SNF conditions. Cells heavily colonized by bacteroids are shown as electron-dense areas. Bars = 250  $\mu\text{m}$ . (B) Electron micrographs of cells colonized with differentiated elongated bacteroids in the nitrogen fixation zone of nodules from EV control and RNAi plants grown for 28 d under SNF condition. Bars = 10  $\mu\text{m}$ . (C) The distribution of bacteroid size measured in electron micrographs of infected cells in the nitrogen-fixing zone. For both nodules from EV control and RNAi plants, the size of 1,000 bacteroids was measured from 30 to 40 distinct cells.

no decrease in shoot Pi content, the typical phenotype of null *pho1* mutants in *A. thaliana*, rice, and tomato (Poirier et al., 1991; Secco et al., 2010; Zhao et al., 2019), it is likely that other members of the *MtPHO1* gene family expressed in the root vascular cylinder contribute to this activity, including *MtPHO1.1* and *MtPHO1.3*. Analysis of higher order knock-out mutants for these genes should help clarify their respective contribution to long-distance, root-to-shoot Pi transport.

The concomitant downregulation of *MtPHO1.1* and *MtPHO1.2* in nodules by RNAi led to a  $\sim 3.5$ -fold reduction in nitrogen fixation in nodules. This significantly impacted growth of plants relying on nitrogen fixation as the primary source of usable N. Interestingly, neither the knocked-down or null *Tnt1* mutants in *MtPHO1.1* or *MtPHO1.2*, respectively, showed growth phenotypes or perturbations in Pi content in nodules in plants grown under SNF conditions. These results would suggest that these genes are likely to have redundant function in nodules. The similar expression profiles of these two genes in nodules and the ability of the respective proteins to mediate Pi export when expressed in *N. benthamiana* supports this conclusion. However, the observation that the majority of *MtPHO1.1* and *MtPHO1.2* proteins are not localized in the same sub-cellular membrane when expressed in *N. benthamiana* raises the possibility that, whereas both proteins contribute to nodule Pi homeostasis and SNF, their mode of action is not completely redundant (see further discussion on *MtPHO1.1* and *MtPHO1.2* localization below).

Whereas shoot Pi content was not affected in RNAi plants compared to EV controls, irrespective of the growth conditions, nodule Pi content was decreased by  $\sim$ two-fold in RNAi plants.

Experiments with  $^{33}\text{P}$ i showed that the transfer of Pi acquired by nodules into the bacteroids was significantly decreased, despite that direct Pi uptake from the bathing medium into nodules was not affected in the RNAi plants. These data support the hypothesis that *MtPHO1.1* and *MtPHO1.2* expression in nodules directly contributes to Pi transfer from the plant cells to the bacteroids. No perturbation in the transfer of  $\text{SO}_4$  from the nodule cells to the bacteroids was observed, in agreement with the specificity of PHO1 for Pi export (Arpat et al., 2012; Wege et al., 2016). Interestingly, RNAi plants showed a 1.5-fold increase in nodule weight although the number of nodules per plant remained the same. The increase in nodule weight in RNAi plants could potentially be a consequence of the reduction of SNF. Previous studies have shown that under nitrogen deficit, symbiotic plants can stimulate nodule expansion via a systemic signal as a compensatory mechanism aimed at increasing nitrogen acquisition capacities (Jeudy et al., 2010; Laguerre et al., 2012).

Pi transport in *S. meliloti* is mediated by both low-affinity Pit- and high-affinity Pst transporters. As in *Escherichia coli*, the Pit-encoding gene *OrfA* is strongly expressed under Pi-sufficient conditions but repressed under Pi-deficient conditions. Conversely, the PstSCAB operon involved in high-affinity Pi transport is repressed under Pi-sufficient conditions but induced under Pi starvation (Bardin et al., 1998; Yuan et al., 2006; diCenzo et al., 2017). Relative expression of the Pit- and Pst-encoding operons in bacteroids has previously been used to deduce the level of Pi availability in indeterminate nodules, e.g. in *M. truncatula*, and determinate nodules, e.g. soybean (Bardin et al., 1998; Yuan et al., 2006; diCenzo et al., 2017; Hu et al., 2018). In the present study,

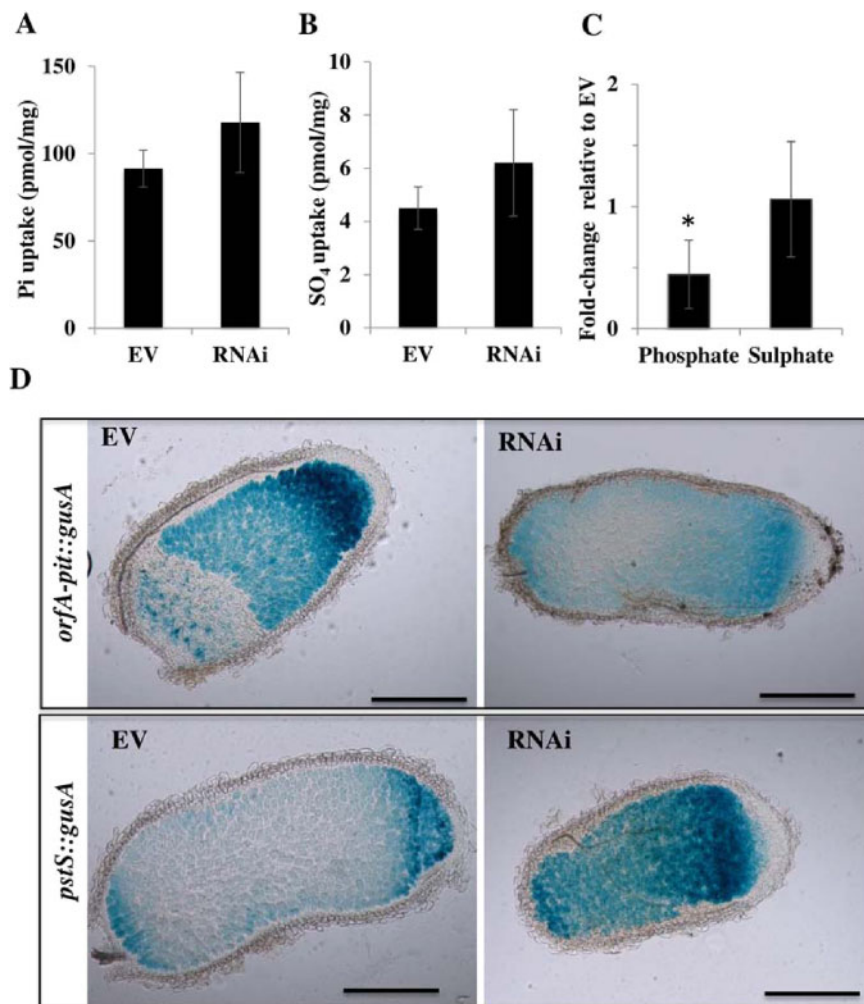


**Figure 6** Flux of Pi and SO<sub>4</sub> into nodules and bacteroids. Isolated nodules from EV control plants and RNAi plants grown in clay-based substrate under SNF conditions were incubated in a nutrient solution containing either <sup>33</sup>Pi (A) or <sup>35</sup>SO<sub>4</sub> (B) and the amount of <sup>33</sup>Pi and <sup>35</sup>SO<sub>4</sub> absorbed by the nodule was measured. Error bars represent SD ( $n = 4$ ). (C) The amount of <sup>33</sup>Pi and <sup>35</sup>SO<sub>4</sub> acquired by bacteroids in the RNAi line was normalized to the number of bacteroids and expressed relative to the EV control. Error bars represent SD ( $n = 4$ ). Asterisks represent statistically significant differences for RNAi compared to the EV control ( $t$  test,  $P < 0.05$ ). (D) Cross-section of nodules stained for  $\beta$ -glucuronidase activity taken from RNAi and EV plants infected with *S. meliloti* strain Sm2011 harboring the promoter fusion *orfA::gusA* or *pstS::gusA* and grown under SNF conditions. Bars = 500  $\mu$ m.

bacteroids containing the *OrfA::gusA* reporter showed a reduction in expression in nodules of the *PHO1* RNAi plants compared to the control, whereas the reverse was observed for bacteroids containing the *Pst::gusA* reporter. These data show that the reduction of *MtPHO1.1* and *MtPHO1.2* expression in nodules leads to an activation of the Pi-starvation response in bacteroids, consistent with the lower level of Pi transfer from the nodule plant cells to bacteroids. Nodules are metabolically highly active and bacteroids fixing nitrogen contain high amount of Pi, ATP, and other phosphorylated intermediates (Gaude et al., 2004; Vauclare et al., 2013). Rhizobium mutants affected in the expression of Pi importers show defect in nodulation and SNF, highlighting the importance of an adequate supply of Pi to bacteroids for optimal SNF (Bardin et al., 1996; Jiao et al., 2016; Hu et al., 2018). Taken together, these data indicate that the reduction of Pi supply from the plant nodule to the bacteroids is

likely to be the primary effect of the downregulation of *MtPHO1.1* and *MtPHO1.2* expression, which in turn negatively impacts nitrogen fixation and nodulation. It is unknown whether Pi-deficiency in bacteroids causes a reduction in bacteroid size or whether other more indirect effect are involved, such as changes in the expression of nodule-specific cysteine-rich peptides (NCRs) known to affect bacteroid differentiation and size (Horvath et al., 2015)

*Arabidopsis thaliana* PHO1 is primarily localized to the Golgi and *trans*-Golgi network (TGN) either when expressed under control of its native promoter in the root vascular cylinder or under control of the CaMV35S promoter in *N. benthamiana* leaves, and this expression pattern is concomitant with its Pi export activity to the apoplast (Arpat et al., 2012; Liu et al., 2012). The absence of detectable amounts of AtPHO1 at the PM could be part of a post-translational retrieval mechanism to control its activity. This would be

analogous to IRT1, an iron transporter that acts at the PM but partitions primarily to the endomembrane system, which is part of a mechanism to control iron import through constitutive IRT1 endocytosis regulated via monoubiquitin- and clathrin-dependent mechanisms (Barberon et al., 2011). We have been unable to detect expression of MtPHO1.1-GFP or MtPHO1.2-GFP in nodules, likely due to the combination of weak expression and high level of tissue autofluorescence. However, functional expression in *N. benthamiana* showed that Pi export activity was associated with PM and Golgi localization of MtPHO1.1-GFP and MtPHO1.2-GFP, respectively. Although it is unknown whether MtPHO1.1 and MtPHO1.2 have distinct subcellular localizations within nodules, these results in *N. benthamiana* show that Pi export mediated by MtPHO1.1 and MtPHO1.2 is not constrained by their predominant steady-state sub-cellular localization either at the PM or Golgi. These results imply that the distinct subcellular localization of MtPHO1.1 and MtPHO1.2 at steady-state levels may not necessarily reflect distinct modes of action as Pi exporters, but perhaps distinct modes of regulation. For example, whereas both Pi exporters would transit via the Golgi–TGN–exocytic vesicle pathway to reach their final destination, MtPHO1.2 would be more partitioned, at steady-state level, in the Golgi–TGN (similar to IRT1), while MtPHO1.1 would be more partitioned to the PM (or SM in nodules).

Transfer of Pi from the cytoplasm of infected plant nodule cells to the bacteroids must ultimately occur across the SM, which acts as the gate keeper to the bacteroids (Roy et al., 2020). A proteomic study aimed at identifying SM proteins in soybean reported the presence of the Pi transporters GmPT5 (Glyma10g04230) and GmPT7 (Glyma10g33030), both belonging to the PHT1 family (Clarke et al., 2015). However, further studies of these proteins found them expressed either in the nodule vascular bundle for GmPT5 (Qin et al., 2012), or the PM of cells of the nodule outer cortex and fixation zones for GmPT7 (Chen et al., 2019), making them unlikely candidates for SM Pi transporters. Although the present work demonstrates the implication of MtPHO1.1 and MtPHO1.2 in the transfer of Pi transfer from the nodule cells to the bacteroids, further work is necessary to elucidate more precisely their mode of action. In particular, it will be interesting to determine if MtPHO1.1 and/or MtPHO1.2 can be localized at the SM, either at steady-state level or transiently. It will also be interesting to determine whether the sub-cellular localization of MtPHO1.1 and MtPHO1.2 is distinct between infected cells of nodules and cells of the vascular cylinder.

## Materials and methods

### Identification of PHO1 family members in *M. truncatula*

*Medicago truncatula* PHO1 genes were identified by sequence similarity to the complete *A. thaliana* PHO1 using the TBLASTN algorithm at the *M. truncatula* Genome Database (<http://blast.jcvi.org/Medicago-Blast/index.cgi>) and the Noble Foundation *Medicago truncatula* IMGAG V3.0 (<https://gb.noble.org/cgi-bin/gb2/gbrowse/medicago>). The

gene nomenclature and associated annotation numbers are given in Supplemental Figure S1. The phylogenetic tree was constructed through the MABL bioinformatics platform (<https://www.phylogeny.fr>; Dereeper et al., 2008).

### Plant material, bacterial strains, growth conditions, and hairy root transformation

*Medicago truncatula* plants were derived from the ecotypes A17 and R108, whereas the *S. meliloti* strain was Rm2011. The *M. medicago* *Tnt1* mutant population (Tadege et al., 2008) was screened for insertions in the *MtPHO1.1* and *MtPHO1.2* genes by PCR as previously described (Cheng et al., 2011). Oligonucleotide sequences used as primers for PCR and genotyping are provided in Supplemental Table S1.

Seeds were scarified for 10 min in H<sub>2</sub>SO<sub>4</sub>, rinsed five times with sterile water, followed by surface sterilization for 10 min with 33% (v/v) commercial bleach. Seeds were then rinsed five times with sterile water and left in the dark in 50-mL tubes for 1 h to imbibe. Surface-sterilized seeds were placed on inverted plates containing 0.7% (w/v) agarose in the dark for 3 d at 4°C and 1 d at 20°C. Germinated seedlings were transferred to agar-solidified Fahræus medium (0.132 g/L CaCl<sub>2</sub>, 0.12 g/L MgSO<sub>4</sub>·7H<sub>2</sub>O, 0.1 g/L KH<sub>2</sub>PO<sub>4</sub>, 0.075 g/L Na<sub>2</sub>HPO<sub>4</sub>·2H<sub>2</sub>O, 5 mg/L Fe-citrate, and 0.07 mg/L each of MnCl<sub>2</sub>·4H<sub>2</sub>O, CuSO<sub>4</sub>·5H<sub>2</sub>O, ZnCl<sub>2</sub>, H<sub>3</sub>BO<sub>3</sub>, and Na<sub>2</sub>MoO<sub>4</sub>·2H<sub>2</sub>O, adjusted to pH 6.5 before autoclaving) and grown for 10 d for hairy root transformation using *Agrobacterium rhizogenes* ARqua1 essentially as previously described (Boisson-Dernier et al., 2001). Following hairy root transformation, seedlings were grown vertically on Fahræus medium supplemented with 25 µg·mL<sup>-1</sup> kanamycin in a growth chamber at 21°C (16 h light/8 h dark cycles) for 14 d, before being transferred to pots in a clay-based substrate (Seramis; <https://www.seramis.com/>) with no additional fertilizer. Seven days after transfer to pots, plants were inoculated with *S. meliloti* grown in TY medium (Beringer, 1974) and resuspended in nitrogen-free, half-strength B&D medium (Broughton and Dilworth, 1971) to an optical density at 600 nm (OD<sub>600</sub>) of 0.02. Each plant was supplied with 50 mL of the inoculum at the base of the stem. Inoculation with *S. meliloti* was repeated after 10 d.

Noninoculated control plants were grown in the clay-based substrate fertilized every 10 d with nitrogen-free half-strength B&D medium (Broughton and Dilworth, 1971) containing 3 mM of KNO<sub>3</sub> and 2.5 mM NH<sub>4</sub>NH<sub>3</sub>, whereas plants grown under nitrogen fixation conditions were fertilized with a similar nutrient solution but without any source of nitrogen. Plants were grown in a greenhouse with a 16 h, 25°C light/8 h, 20°C dark cycle.

### RNA preparation and RT-qPCR

Plant tissues were frozen in liquid nitrogen, then ground using a mortar and pestle and the powder was used to extract the RNA using the RNeasy Plant Mini Kit (Qiagen). Samples were treated with DNase on columns during the RNA extraction using the RNase-free DNase kit (Qiagen). RNA samples were used for reverse transcription using SuperScript II

reverse transcriptase (Invitrogen). qPCR was performed using SYBER Select Master Mix (Invitrogen) and the Stratagene Mx3005 qPCR system using gene-specific primer (Supplemental Table S2).

### Generation of PHO1-GUS fusion genes and GUS staining

Plasmid pMDC163 (Curtis and Grossniklaus, 2003) was digested by restriction enzyme *Xho*I to excise the hygromycin-resistance cassette to replace it with the neomycin phosphotransferase cassette amplified from plasmid pMDC100 (Curtis and Grossniklaus, 2003) and inserted by In-Fusion (Takara Bio). The modified pMDC163 plasmid was named pMDC163K. A 2-kb DNA fragment upstream of the starting ATG of *MtPHO1.1* (*Medtr1g041695.1*), *MtPHO1.2* (*Medtr1g075640.1*), or *MtPHO1.3* (*Medtr8g069955.1*) was amplified by PCR using gene-specific primers (Supplemental Table S3) from genomic DNA of *M. truncatula* A17, whereas the coding sequence of genes was amplified by PCR using gene-specific primers (Supplemental Table S3) from cDNA derived from whole plants. The promoter and coding cDNA fragments were cloned into the pENTR2B (Invitrogen) by In-Fusion, checked by sequencing and then fused to the *GUS* reporter gene in the destination vector pMDC163K or pKGWFS7-RR (Karimi et al., 2002) by In-Fusion (Takara Bio). The various DNA constructs were introduced in plants via hairy root transformation using *A. rhizogenes* ARqua1, as described above. Nodules were stained for GUS activity by infiltrating, under mild vacuum, a solution containing 2 mM 5-bromo-4-chloro-3-indolyl- $\beta$ -glucuronic acid (X-Gluc), 10 mM EDTA, 2 mM potassium ferricyanide, 2 mM potassium ferrocyanide, 0.1% (v/v) Triton X-100, and 100 mM sodium Pi, pH 7. The enzymatic reaction was performed at 37°C in the dark. Stained tissues were washed with a graded ethanol series [10%–80% {v/v}] and cleared in chloral hydrate solution [2.7 g·mL<sup>-1</sup> in 30% {v/v} glycerol].

### Expression of MtPHO1-GFP fusion in *N. benthamiana*, ion export and confocal analysis

The *MtPHO1.1* and *MtPHO1.2* genes were amplified from genomic DNA using gene-specific primers (Supplemental Table S3), cloned into the pENTR2B (Invitrogen) by In-Fusion polymerase (Takara Bio), and inserted into pMDC83 plasmid by Gateway cloning (Invitrogen). For transient expression, *N. benthamiana* plants were infiltrated with *Agrobacterium tumefaciens* as previously described (Arpat et al., 2012). Pi and nitrate export assays were performed as previously described (Arpat et al., 2012). Pi concentration in solution was quantified by the molybdate assay (Ames, 1966), whereas nitrate was quantified by first converting nitrate to nitrite using commercial nitrate reductase from *Aspergillus niger* (Sigma) followed by nitrite quantification using sulfanilamide (Barthes et al., 1995). Confocal imaging was performed using a Zeiss LSM 700 instrument with Aplanachromat 63 × NA1.2 water immersion or multi-immersion objective.

### Generation of RNAi construct

RNAi construct were designed by fusing together PCR fragments from *MtPHO1.1* and *MtPHO1.2* by In-Fusion (Takara Bio) and cloning the product in pENTR2B. The chimeric fragments were inserted into pK7GWIWG5D(II) harboring the promoter of the *MtNCR001* gene (Mergaert et al., 2003) using Gateway Technology (Invitrogen). Sequences of oligonucleotides used for this cloning are listed in Supplemental Table S4.

### Nitrogen fixation assay

The <sup>15</sup>N<sub>2</sub> fixation was measured essentially as previously described (Ruffel et al., 2008). Freshly excised nodulated roots were placed in air-tight, 10-mL tubes containing 2 mL of basal nutrient solution. Ten minutes labeling was achieved by replacing in each tube 5 mL of air by 5 mL of 80%<sup>15</sup>N<sub>2</sub>/20%O<sub>2</sub> mix (99 atom% <sup>15</sup>N). Samples (100  $\mu$ L) of <sup>15</sup>N<sub>2</sub>-enriched air were harvested at the beginning and at the end of the labeling, for precise analysis of the atom % <sup>15</sup>N of the <sup>15</sup>N<sub>2</sub> source and leak check. After labeling, nodules were separated from roots, both organs were dried and analyzed for <sup>15</sup>N and total N contents using a continuous-flow isotope ratio mass spectrometer (Isoprime mass spectrometer, GV instruments) coupled to a nitrogen elemental analyzer (Euro vector S.P.A) at the stable isotope platform of B&PMP (<https://www1.montpellier.inra.fr/wp-inra/bpmp/en/plateform/stable-isotope-analytical-platform/>). N<sub>2</sub> fixation capacity was expressed as the number of  $\mu$ mole of N atoms acquired per g of nodule dry weight and hours.

### <sup>33</sup>PO<sub>4</sub> and <sup>35</sup>SO<sub>4</sub> flux measurement in nodules

Nodules from transgenic roots were harvested, weighed, and placed in a solution containing 10  $\mu$ M KH<sub>2</sub>PO<sub>4</sub>, 10  $\mu$ M Mg<sub>2</sub>SO<sub>4</sub>, 100  $\mu$ M CaCl<sub>2</sub>, and 1 mM KCl, pH 5.6 and supplemented with either 10  $\mu$ Ci/mL of <sup>33</sup>PO<sub>4</sub> or <sup>35</sup>SO<sub>4</sub>. After 8 h, nodules were washed extensively with the same solution without radioisotopes, and total radioactivity in nodules measured by crushing nodules and adding 5 mL of scintillation cocktail (Ultima Gold, Perkin Elmer). To measure the uptake of <sup>33</sup>PO<sub>4</sub> or <sup>35</sup>SO<sub>4</sub> into bacteroids, the nodules were crushed in ice-cold bacteroid extraction buffer (BEB = 125 mM KCl, 50 mM Na-succinate, 50 mM N-[Tris(hydroxymethyl)-methyl]-2-aminoethanesulfonic acid (TES), pH7.0) containing 1% (w/v) bovine serum albumin (BSA). The slurry was first centrifuged at 100g for 10 min to remove plant debris and the suspension was then centrifuged at 3,600g for 20 min at 4°C. The pellet was resuspended in ice-cold BEB at OD<sub>600</sub> = 1, loaded on top of a 70% (v/v) percoll solution in BEB buffer and centrifuged for 30 min at 48,000g at 4°C. The band containing bacteroids was carefully removed by pipetting, diluted in 1.4 mL of ice-cold BEB and centrifuged at 3,600g for 10 min at 4°C. The pellet representing a purified bacteroid preparation was resuspended in a small volume of ice-cold BEB. A portion was mixed with scintillation cocktail for radioactivity measurement, whereas another portion was examined by microscopy to count the number of bacteroids per volume.

The amount of  $^{33}\text{PO}_4$  or  $^{35}\text{SO}_4$  measured was then normalized to the amount of bacteroids in the solution. Radioactivity was measured in the Perkin Elmer tri-carb 2800TR Scintillation counter.

### Electron and light microscopy

Nodules were fixed in a 2.5% (w/v) glutaraldehyde solution (EMS) in 0.1 M Pi buffer (PB; pH 7.4) for 12 h at RT under vacuum. They were then washed several times in PB, and post-fixed in a fresh mixture of osmium tetroxide 1% (w/v; EMS) with 1.5% (w/v) of potassium ferrocyanide in PB buffer for 3 h at RT under vacuum. The samples were then washed twice in distilled water and dehydrated in a graded acetone solution. This was followed by infiltration in LR White resin (EMS) and finally polymerized for 48 h at 60°C in an oven under nitrogen atmosphere. Semi-thin sections 200- $\mu\text{m}$  thick (for light microscopy) and ultrathin sections 50-nm thick (for TEM microscopy) were cut longitudinally in the middle of the nodule using a Leica Ultracut (Leica Mikrosysteme GmbH) and picked up on cover glass (for light microscopy) or a copper slot grid  $2 \times 1 \text{ mm}^2$  (for TEM microscopy) coated with a polystyrene film (Sigma). Ultrathin sections were post-stained with 4% (w/v) uranyl acetate (Sigma) in water for 10 min, rinsed several times with water followed by Reynolds lead citrate in water (Sigma) for 10 min and rinsed several times with water.

Micrographs were taken with a transmission electron microscope FEI CM100 (FEI, Eindhoven, The Netherlands) at an acceleration voltage of 80 kV with a TVIPS TemCamF416 digital camera (TVIPS GmbH, Gauting, Germany). For light imaging, micrographs were taken using a Zeiss Axio Imager Z2 (Zeiss, Oberkochen, Germany) with a Hamamatsu digital camera C11440 (Hamamatsu Photonics K.K., Hamamatsu, Japan).

### In situ GUS expression in *S. meliloti*

*Sinorhizobium meliloti* strain Rm2011 containing the plasmids *orf-pit::gusA* and *pstS::gusA* (Yuan et al., 2006) were obtained from T. M. Finan (University of McMaster, Canada) and used to infect plants transformed with EV or the RNAi3 construct. Nodules from transgenic roots of plants grown under SNF conditions were fixed in 3% (w/v) paraformaldehyde under vacuum, stained for GUS activity as described above, embedded in 6% (w/v) agarose, and cut at 100- $\mu\text{m}$  thickness using a vibratome.

### Quantification and statistical analysis

Values are presented as mean  $\pm$  sd. Student's *t* test was used for statistical analyses, with  $P < 0.05$  considered significant. The number of replicates for all experiments is indicated in the figure legends.

### Accession numbers

Sequence data from this article can be found in the GenBank/EMBL data libraries under accession numbers listed in [Supplemental Figure S1](#).

## Supplemental data

The following materials are available in the online version of this article.

**Supplemental Figure S1** Nomenclature and structure of the *M. truncatula* PHO1 gene family.

**Supplemental Figure S2** Expression pattern of the *MtPHO1* genes.

**Supplemental Figure S3** Analysis of plants with composite transgenic roots transformed with RNAi constructs targeting the *MtPHO1.1* and *MtPHO1.2* genes.

**Supplemental Figure S4** Sequence of the three RNAi constructs used to downregulate *MtPHO1.1* and *MtPHO1.2* genes.

**Supplemental Table S1** Gene-specific primer pairs used in *Tnt1* mutant genotyping.

**Supplemental Table S2** Gene-specific primer pairs used in RT-PCR analysis.

**Supplemental Table S3** Gene-specific primer pairs used in making gMtPHO1 MtPHO1::GUS fusions.

**Supplemental Table S4** Gene-specific primer pairs used in RNAi constructs.

## Acknowledgments

We are very grateful to F. Turlough (McMaster University) for providing the *S. meliloti* strains containing *orfA-pit::lacZ* and *pstS::lacZ*. We also thank P. Tillard for  $^{15}\text{N}$  measurements at the Stable Isotope Platform of B&PMP (Montpellier, France) and Peter Mergaert (Paris-Saclay) for help with the isolation of bacteroids.

## Funding

This study was supported by a grant from the Swiss-South African Joint Research Program (SSAJRP; project number IZLSZ3 148854) to Y.P. and A.J.V., and a grant from the Swiss National Science Foundation (31003A\_159998) to Y.P.

*Conflict of interest statement.* None declared.

## References

- Al-Niemi TS, Kahn ML, McDermott TR (1998) Phosphorus uptake by bean nodules. *Plant Soil* **198**: 71–78
- Ames BN (1966) Assay of inorganic phosphate, total phosphate and phosphatases. *Methods Enzymol* **8**: 115–118
- Arpat AB, Magliano P, Wege S, Rouached H, Stefanovic A, Poirier Y (2012) Functional expression of PHO1 to the Golgi and trans-Golgi network and its role in export of inorganic phosphate. *Plant J* **71**: 479–491
- Barberon M, Zelazny E, Robert S, Conéjéro G, Curie C, Friml J, Vert G (2011) Monoubiquitin-dependent endocytosis of the IRON-REGULATED TRANSPORTER 1 (IRT1) transporter controls iron uptake in plants. *Proc Natl Acad Sci USA* **108**: E450–E458
- Bardin S, Dan S, Osteras M, Finan TM (1996) A phosphate transport system is required for symbiotic nitrogen fixation by *Rhizobium meliloti*. *J Bacteriol* **178**: 4540–4547
- Bardin SD, Voegelé RT, Finan TM (1998) Phosphate assimilation in *Rhizobium* (*Sinorhizobium*) *meliloti*: identification of a pit-like gene. *J Bacteriol* **180**: 4219–4226

- Barthes L, Bousser A, Hoarau J, Deleens E (1995) Reassessment of the relationship between nitrogen supply and xylem exudation in detopped maize seedlings. *Plant Physiol Biochem* **33**: 173–183
- Batistič O, Waadt R, Steinhörst L, Held K, Kudla J (2010) CBL-mediated targeting of CIPKs facilitates the decoding of calcium signals emanating from distinct cellular stores. *Plant J* **61**: 211–222
- Beringer JE (1974) R factor transfer in *Rhizobium leguminosarum*. *J Gen Microbiol* **84**: 188–198
- Boisson-Dernier A, Chabaud M, Garcia F, Becard G, Rosenberg C, Barker DG (2001) *Agrobacterium rhizogenes*-transformed roots of *Medicago truncatula* for the study of nitrogen-fixing and endomycorrhizal symbiotic associations. *Mol Plant-Microbe Interact* **14**: 695–700
- Botero LM, Al-Niemi TS, McDermott TR (2000) Characterization of two inducible phosphate transport systems in *Rhizobium tropici*. *Appl Environ Microbiol* **66**: 15–22
- Broughton WJ, Dilworth MJ (1971) Control of leghaemoglobin synthesis in snake beans. *Biochem J* **125**: 1075–+
- Chen LY, Qin L, Zhou LL, Li XX, Chen ZC, Sun LL, Wang WF, Lin ZH, Zhao J, Yamaji N, et al. (2019) A nodule-localized phosphate transporter GmPT7 plays an important role in enhancing symbiotic N<sub>2</sub> fixation and yield in soybean. *New Phytol* **221**: 2013–2025
- Cheng X, Wen J, Tadege M, Ratet P, Mysore KS (2011) Reverse genetics in *Medicago truncatula* using Tnt1 insertion mutants. *Methods Mol Biol* **678**: 179–190
- Clarke VC, Loughlin PC, Day DA, Smith PMC (2014) Transport processes of the legume symbiosome membrane. *Front Plant Sci* **5**: 699
- Clarke VC, Loughlin PC, Gavrin A, Chen C, Brear EM, Day DA, Smith PMC (2015) Proteomic analysis of the soybean symbiosome identifies new symbiotic proteins. *Mol Cell Proteom* **14**: 1301–1322
- Curtis MD, Grossniklaus U (2003) A gateway cloning vectors set for high-throughput functional analysis of genes in planta. *Plant Physiol* **133**: 462–469
- Dereeper A, Guignon V, Blanc G, Audic S, Buffet S, Chevenet F, Dufayard JF, Guindon S, Lefort V, Lescot M, et al. (2008) Phylogeny.fr: robust phylogenetic analysis for the non-specialist. *Nucleic Acids Res* **36**: W465–W469
- diCenzo GC, Sharthiya H, Nanda A, Zamani M, Finan TM (2017) PhoU allows rapid adaptation to high phosphate concentrations by modulating PstSCAB transport rate in *Sinorhizobium meliloti*. *J Bacteriol* **199**: e00143–17
- Gaude N, Tippmann H, Fletmetakis E, Katinakis P, Udvardi M, Dormann P (2004) The galactolipid digalactosyldiacylglycerol accumulates in the peribacteroid membrane of nitrogen-fixing nodules of soybean and *Lotus*. *J Biol Chem* **279**: 34624–34630
- Gunawardena S, Danso SKA, Zapata F (1992) Phosphorus requirements and nitrogen accumulation by 3 mungbean (*Vigna radiata* (L) *welz*) cultivars. *Plant Soil* **147**: 267–274
- Hamburger D, Rezzonico E, MacDonald-Comber Petétot J, Somerville C, Poirier Y (2002) Identification and characterization of the *Arabidopsis* PHO1 gene involved in phosphate loading to the xylem. *Plant Cell* **14**: 889–902
- He L, Zhao M, Wang Y, Gai J, He C (2013) Phylogeny, structural evolution and functional diversification of the plant PHOSPHATE1 gene family: a focus on *Glycine max*. *BMC Evol Biol* **13**: 103
- Hernandez G, Valdes-Lopez O, Ramirez M, Goffard N, Weiller G, Aparicio-Fabre R, Fuentes SI, Erban A, Kopka J, Udvardi MK, et al. (2009) Global changes in the transcript and metabolic profiles during symbiotic nitrogen fixation in phosphorus-stressed common bean plants. *Plant Physiol* **151**: 1221–1238
- Herridge DF, Peoples MB, Boddey RM (2008) Global inputs of biological nitrogen fixation in agricultural systems. *Plant Soil* **311**: 1–18
- Horvath B, Domonkos A, Kereszt A, Szucs A, Abraham E, Ayaydin F, Boka K, Chen Y, Chen R, Murray JD, et al. (2015) Loss of the nodule-specific cysteine rich peptide, NCR169, abolishes symbiotic nitrogen fixation in the *Medicago truncatula* dnf7 mutant. *Proc Natl Acad Sci USA* **112**: 15232–15237
- Hu Y, Jiao J, Liu LX, Sun YW, Chen WF, Sui XH, Chen WX, Tian CF (2018) Evidence for phosphate starvation of rhizobia without terminal differentiation in legume nodules. *Mol Plant-Microbe Interact* **31**: 1060–1068
- Israel DW (1987) Investigation of the role of phosphorus in symbiotic dinitrogen fixation. *Plant Physiol* **84**: 835–840
- Israel DW (1993) Symbiotic dinitrogen fixation and host-plant growth during development of and recovery from phosphorus deficiency. *Physiol Plant* **88**: 294–300
- Jabnour M, Secco D, Lecampion C, Robaglia C, Shu Q, Poirier Y (2013) A rice cis-natural antisense RNA acts as a translational enhancer for its cognate mRNA and contributes to phosphate homeostasis and plant fitness. *Plant Cell* **25**: 4166–4182
- Jedy C, Ruffel S, Freixes S, Tillard P, Santoni AL, Morel S, Journet EP, Duc G, Gojon A, Lepetit M, et al. (2010) Adaptation of *Medicago truncatula* to nitrogen limitation is modulated via local and systemic nodule developmental responses. *New Phytol* **185**: 817–828
- Jiao J, Wu LJ, Zhang BL, Hu Y, Li Y, Zhang XX, Guo HJ, Liu LX, Chen WX, Zhang ZD, et al. (2016) MucR is required for transcriptional activation of conserved ion transporters to support nitrogen fixation of *Sinorhizobium fredii* in soybean nodules. *Mol Plant-Microbe Interact* **29**: 352–361
- Kaiser BN, Moreau S, Castelli J, Thomson R, Lambert A, Bogliolo S, Puppo A, Day DA (2003) The soybean NRAMP homologue, GmDMT1, is a symbiotic divalent metal transporter capable of ferrous iron transport. *Plant J* **35**: 295–304
- Kang X, Ni M (2006) Arabidopsis SHORT HYPOCOTYL UNDER BLUE1 contains SPX and EXS domains and acts in cryptochrome signaling. *Plant Cell* **18**: 921–934
- Karimi M, Inze D, Depicker A (2002) GATEWAY(TM) vectors for *Agrobacterium*-mediated plant transformation. *Trends Plant Sci* **7**: 193–195
- Khan GA, Bouraine S, Wege S, Li Y, de Carbonnel M, Berthomieu P, Poirier Y, Rouached H (2014) Coordination between zinc and phosphate homeostasis involves the transcription factor PHR1, the phosphate exporter PHO1, and its homologue PHO1;H3 in *Arabidopsis*. *J Exp Bot* **65**: 871–884
- Krusell L, Krause K, Ott T, Desbrosses G, Kramer U, Sato S, Nakamura Y, Tabata S, James EK, Sandal N, et al. (2005) The sulfate transporter SST1 is crucial for symbiotic nitrogen fixation in *Lotus japonicus* root nodules. *Plant Cell* **17**: 1625–1636
- Kryvoruchko IS, Routray P, Sinharoy S, Torres-Jerez I, Tejada-Jimenez M, Finney LA, Nakashima J, Pislariu CI, Benedito VA, Gonzalez-Guerrero M, et al. (2018) An iron-activated citrate transporter, MtMATE67, is required for symbiotic nitrogen fixation. *Plant Physiol* **176**: 2315–2329
- Laguette G, Heulin-Gotty K, Brunel B, Klonowska A, Le Quere A, Tillard P, Prin Y, Cleyet-Marel JC, Lepetit M (2012) Local and systemic N signaling are involved in *Medicago truncatula* preference for the most efficient *Sinorhizobium* symbiotic partners. *New Phytol* **195**: 437–449
- Langhans M, Forster S, Helmchen G, Robinson D (2011) Differential effects of the brefeldin A analogue (6R)-hydroxy-BFA in tobacco and *Arabidopsis*. *J Exp Bot* **62**: 2949–2957
- Liu T-Y, Huang T-K, Tseng C-Y, Lai Y-S, Lin S-I, Lin W-Y, Chen J-W, Chiou T-J (2012) PHO2-dependent degradation of PHO1 modulates phosphate homeostasis in *Arabidopsis*. *Plant Cell* **24**: 2168–2183
- McKay IA, Djordjevic MA (1993) Production and excretion of nod metabolites by *Rhizobium leguminosarum* bv *trifolii* are disrupted by the same environmental factors that reduce nodulation in the field. *Appl Environ Microbiol* **59**: 3385–3392
- Mergaert P, Kereszt A, Kondorosi E (2020) Gene expression in nitrogen-fixing symbiotic nodule cells in *Medicago truncatula* and other nodulating plants. *Plant Cell* **32**: 42–68

- Mergaert P, Nikovics K, Kelemen Z, Maunoury N, Vaubert D, Kondorosi A, Kondorosi E** (2003) A novel family in *Medicago truncatula* consisting of more than 300 nodule-specific genes coding for small, secreted polypeptides with conserved cysteine motifs. *Plant Physiol* **132**: 161–173
- Moreau S, Thomson RM, Kaiser BN, Trevaskis B, Guerinot ML, Udvardi MK, Puppo A, Day DA** (2002) GmZIP1 encodes a symbiosis-specific zinc transporter in soybean. *J Biol Chem* **277**: 4738–4746
- Nussaume L, Kanno S, Javot H, Marin E, Pochon N, Ayadi A, Nakanishi TM, Thibaud M-C** (2011) Phosphate import in plants: focus on the PHT1 transporters. *Front Plant Sci* **2**: 83
- O'Rourke J, Yang S, Miller S, Bucciarelli B, Liu J, Rydeen A, Bozsoki Z, Uhde-Stone C, Tu Z, Allan D, et al.** (2013) An RNA-Seq transcriptome analysis of orthophosphate-deficient white lupin reveals novel insights into phosphorus acclimation in plants. *Plant Physiol* **161**: 705–724
- Oldroyd GED, Murray JD, Poole PS, Downie JA** (2011) The rules of engagement in the legume-rhizobial symbiosis. *Ann Rev Genetics* **45**: 119–144
- Poirier Y, Jung J-Y** (2015) Phosphate transporters. In **WC Plaxton, H Lambers**, editors, *Phosphorus Metabolism in Plants*, Vol **48**. Wiley, Chichester, UK, pp 125–158
- Poirier Y, Thoma S, Somerville C, Schiefelbein J** (1991) A mutant of *Arabidopsis* deficient in xylem loading of phosphate. *Plant Physiol* **97**: 1087–1093
- Poole P, Ramachandran V, Terpolilli J** (2018) Rhizobia: From saprophytes to endosymbionts. *Nat Rev Microbiol* **16**: 291–303
- Qin L, Zhao J, Tian J, Chen L, Sun Z, Guo Y, Lu X, Gu M, Xu G, Liao H** (2012) The high-affinity phosphate transporter GmPT5 regulates phosphate transport to nodules and nodulation in soybean. *Plant Physiol* **159**: 1634–1643
- Roux B, Rodde N, Jardinaud MF, Timmers T, Sauviac L, Cottret L, Carrere S, Sallet E, Courcelle E, Moreau S, et al.** (2014) An integrated analysis of plant and bacterial gene expression in symbiotic root nodules using laser-capture microdissection coupled to RNA sequencing. *Plant J* **77**: 817–837
- Roy S, Liu W, Nandety RS, Crook A, Mysore KS, Pislariu CI, Frugoli J, Dickstein R, Udvardi MK** (2020) Celebrating 20 years of genetic discoveries in legume nodulation and symbiotic nitrogen fixation (OPEN). *Plant Cell* **32**: 15–41
- Ruffel S, Freixes S, Balzergue S, Tillard P, Jeudy C, Martin-Magniette ML, van der Merwe MJ, Kakar K, Gouzy J, Fernie AR, et al.** (2008) Systemic signaling of the plant nitrogen status triggers specific transcriptome responses depending on the nitrogen source in *Medicago truncatula*. *Plant Physiol* **146**: 2020–2035
- Saalbach G, Erik P, Wienkoop S** (2002) Characterisation by proteomics of peribacteroid space and peribacteroid membrane preparations from pea (*Pisum sativum*) symbiosomes. *Proteomics* **2**: 325–337
- Secco D, Baumann A, Poirier Y** (2010) Characterization of the rice *PHO1* gene family reveals a key role for *OsPHO1;2* in phosphate homeostasis and the evolution of a distinct clade in dicotyledons. *Plant Physiol* **152**: 1693–1704
- Stefanovic A, Ribot C, Rouached H, Wang Y, Chong J, Belbahri L, Delessert S, Poirier Y** (2007) Members of the *PHO1* gene family show limited functional redundancy in phosphate transfer to the shoot, and are regulated by phosphate deficiency via distinct pathways. *Plant J* **50**: 982–994
- Sulieyman S, Tran LSP** (2015) Phosphorus homeostasis in legume nodules as an adaptive strategy to phosphorus deficiency. *Plant Sci* **239**: 36–43
- Tadege M, Wen JQ, He J, Tu HD, Kwak Y, Eschstruth A, Cayrel A, Endre G, Zhao PX, Chabaud M, et al.** (2008) Large-scale insertional mutagenesis using the Tnt1 retrotransposon in the model legume *Medicago truncatula*. *Plant J* **54**: 335–347
- Udvardi M, Poole PS** (2013) Transport and metabolism in legume-Rhizobia symbioses. *Ann Rev Plant Biol* **64**: 781–805
- Valentine AJ, Kleinert A, Benedito VA** (2017) Adaptive strategies for nitrogen metabolism in phosphate deficient legume nodules. *Plant Sci* **256**: 46–52
- Vauclare P, Bligny R, Gout E, Widmer F** (2013) An overview of the metabolic differences between *Bradyrhizobium japonicum* 110 bacteria and differentiated bacteroids from soybean (*Glycine max*) root nodules: an in vitro <sup>13</sup>C- and <sup>31</sup>P-nuclear magnetic resonance spectroscopy study. *FEMS Microbiol Lett* **343**: 49–56
- Vincill ED, Szczyglowski K, Roberts DM** (2005) GmN70 and LjN70. Anion transporters of the symbiosome membrane of nodules with a transport preference for nitrate. *Plant Physiol* **137**: 1435–1444
- Vogiatzaki E, Baroux C, Jung JY, Poirier Y** (2017) PHO1 exports phosphate from the chalazal seed coat to the embryo in developing *Arabidopsis* seeds. *Curr Biol* **27**: 2893
- Wege S, Khan GA, Jung J-Y, Vogiatzaki E, Pradervand S, Aller I, Meyer AJ, Poirier Y** (2016) The EXS domain of PHO1 participates in the response of shoots to phosphate deficiency via a root-to-shoot signal. *Plant Physiol* **170**: 385–400
- Whitehead LF, Day DA** (1997) The peribacteroid membrane. *Physiol Plant* **100**: 30–44
- Wienkoop S, Saalbach G** (2003) Proteome analysis. Novel proteins identified at the peribacteroid membrane from *Lotus japonicus* root nodules. *Plant Physiol* **131**: 1080–1090
- Xu F, Liu Q, Chen L, Kuang J, Walk T, Wang J, Liao H** (2013) Genome-wide identification of soybean microRNAs and their targets reveals their organ-specificity and responses to phosphate starvation. *BMC Genomics* **14**: 66
- Xue YB, Xiao BX, Zhu SN, Mo XH, Liang CY, Tian J, Liao H** (2017) GmPHR25, a GmPHR member up-regulated by phosphate starvation, controls phosphate homeostasis in soybean. *J Exp Bot* **68**: 4951–4967
- Yuan ZC, Zaheer R, Finan TM** (2006) Regulation and properties of PstSCAB, a high-affinity, high-velocity phosphate transport system of *Sinorhizobium meliloti*. *J Bacteriol* **188**: 1089–1102
- Zhang JY, Zhou X, Xu Y, Yao ML, Xie FB, Gai JY, Li Y, Yang SP** (2016) Soybean SPX1 is an important component of the response to phosphate deficiency for phosphorus homeostasis. *Plant Sci* **248**: 82–91
- Zhao P, You Q, Lei M** (2019) A CRISPR/Cas9 deletion into the phosphate transporter SIPHO1;1 reveals its role in phosphate nutrition of tomato seedlings. *Physiol Plant* **167**: 556–563